International Journal of Innovative Computing, Information and Control
Volume **21**, Number **1**, February **2025**

ICIC International ©2025 ISSN 1349-4198
pp. **99–114**

ROBUST CONTROLLER FOR A QUADRATIC BOOST CONVERTER

Said Oucheriah and Abul Azad*

Department of Engineering Technology
Northern Illinois University
DeKalb, Il 60115, USA
soucheria@niu.edu; *Corresponding author: aazad@niu.edu

Received April 2024; revised August 2024

Abstract. *Quadratic boost converters are highly nonlinear, high-order, nonminimum phase systems and bilinear in nature that present challenges to the regulation of their output voltages. In this paper, the uncertainty and disturbance estimator (UDE) scheme is successfully extended to the design of a robust nonlinear controller to tightly regulate the output voltage of the quadratic boost converter. The parameter uncertainties and disturbances are lumped as a signal that is accurately estimated using a low-pass filter. This estimate is then used by the controller to cancel the effect of the disturbances and uncertainties. This methodology forms the basis of the UDE-based controller. Using simulation, the effectiveness of the developed controller is compared with the widely popular proportional integral (PI) and sliding mode cascade controller that has shown excellent features in terms of output tracking abilities, robustness to system uncertainties and disturbances. Experimental results are also presented to validate the effectiveness and robustness of the proposed controller.*

Keywords: Quadratic boost converter, Robust control, Uncertainty and disturbance estimator (UDE)

1. **Introduction.** Nowadays, DC-DC power electronic converters have many industrial applications such as in vehicular electrical systems, in photovoltaic systems, wind energy battery-storage systems and contant power load systems [1-5]. Their wide ranging use in industry has generated an increase interest in the design of stabilizing controllers. When a large voltage step-up ratio is needed in the context of boost-type DC-DC converters, the second order traditional boost converter is no longer practical and numerous high-gain transformer-based and transformer-less based topologies have been developed. Among them, an interesting and attractive topology is the transform-less quadratic boost converter with a single switch which will be the topology chosen in this work.

The design of a controller to regulate the output voltage of a quadratic boost converter presents a challenge since the converter is a nonlinear, high-order and nonminimum phase system. Currently, the basic control strategy involves the use of an inner loop to control the input current and the use of an outer loop to regulate the output voltage. For the inner current loop, the current-programmed control mode is used in [6] and the average current control mode is used in [7]. In both studies, a PI controller is designed for the outer loop voltage. In [8], the quadratic boost converter is presented based on the reduced redundant power processing principle using current-programmed control for the inner loop and a PI for the outer loop. In [9], a hysteresis-based controller is designed with the fast inner current loop using sliding mode control and the slow outer voltage loop using a PI controller. The designed controller offers many advantages such as ease of implementation,

DOI: 10.24507/ijicic.21.01.99

tight output regulation, fast transient response and robustness to parametric uncertainties and large input voltage and load disturbances. However, the controller suffers from variable switching frequency that can cause excessive switching losses with the problem of electromagnetic interference. In [10], two fixed-frequency PWM-based SM controllers are presented with the sliding surface composed of state variables and the integral and double-integral terms of the output state-variable error. These controllers are implemented using the measurements of the current of the output capacitor and the voltages across the two capacitors of the converter and in addition, controller 1 requires the knowledge of the input voltage. The experimental plots depict only step load variations and the robustness to input voltage variations is not tested. In [11], an adaptive current-mode is proposed that uses the estimate of the load conductance to generate the controller for a hybrid-type high-order boost converter and in [12], a modified voltage-mode controller is considered to regulate the output voltage of the single-switch quadratic boost converter. In both studies, the implementation of the controllers requires the knowledge of the input voltage. In [13], the simple adaptive control (SAC) scheme is successfully implemented to regulate the output voltage of the quadratic boost converter. The implementation of the SAC requires only the measurement of the output voltage and its robustness is validated experimentally against step input voltage and load disturbances. In [14], a controller is proposed based on an inner loop with a sliding mode controller for reaching a desired equilibrium state and an outer loop with integral-type controller for assuring robustness against load and input voltage variations and converter parameter uncertainties. The proposed controller also deals with sudden changes in the nominal operating conditions. However, the resulting sliding function designed is a nonlinear function of all the state variables that must be measured. The proposed control law is discontinous and the presence of chattering effects is shown in the experimental plots. In [15], a non-linear robust control law based on the Brunovsky canonical model of the converter is developed in the presence of an unpredictable load with an observer to estimate the output disturbances. The implementation of the controller requires four sensors to measure all the state variables. In [16], a PWM-based current-sensorless robust sliding mode controller for the DC-DC quadratic boost converter is proposed that requires only one sensor for the ouput voltage measurement. An extended state observer is used to estimate a lumped uncertainty signal that comprises the uncertain load and the input voltage and also to estimate the derivative of the output voltage. A linear sliding surface is used to derive the controller that is simple in its design and yet exhibits excellent features in terms of disturbance suppression despite the absence of the inductor current feedback. However, the robustness of the controller is validated only by simulation and no experimental results are provided.

In this work, a fixed-frequency pulsewidth modulation controller is designed to regulate the output of the transform-less quadratic boost converter with a single active switch by successfully extending the uncertainty and disturbance estimator (UDE) scheme [17,18] to a highly nonlinear, high-order, nonminimum phase and bilateral device. The basic idea behind the UDE method is the use of a filter of appropriate bandwidth to estimate a lumped signal composed of system uncertainties and time-varying external disturbances. This methodology yields a simple controller design and does not require any complicated estimation schemes or nonlinear disturbance observers that are designed in the context of adaptive controllers. The contributions of this paper are as follows:

1) Successful extension of the UDE-based controller methodology and its implementation for the quadratic DC-DC boost converter that is a high-order, bilinear in nature and nonminimum phase system;

2) Development of a simple procedure that systematically determines the parameters of the controller to achieve a satisfactory response;

3) Using simulation, the effectiveness of the proposed controller is compared against the widely popular robust sliding mode controller of [9] and its robustness is also validated experimentally.

The structure of this paper is as follows. In Section 2, the quadratic boost converter model is presented. Section 3 introduces the UDE-based controller design and Section 4 presents the stability analysis. Section 5 describes the effects of the controller parameters on the output transient response and presents a procedure for their selections to achieve a satisfactory transient output response. In Section 6, a computer simulation comparison of the proposed controller with the work in [9] is presented. In Section 7, simulation and experimental results are presented to validate the robustness of the proposed controller and finally the conclusion is provided in Section 8.

2. **Quadratic Boost Converter.** A basic quadratic boost converter with a single active switch is shown in Figure 1. Under continuous conduction mode, the averaged model of the converter is

$$\begin{aligned}
\dot{x}_1 &= -(1-u)\frac{x_3}{L_1} + \frac{E}{L_1} \\
\dot{x}_2 &= -(1-u)\frac{x_4}{L_2} + \frac{x_3}{L_2} \\
\dot{x}_3 &= (1-u)\frac{x_1}{C_1} - \frac{x_2}{C_1} \\
\dot{x}_4 &= (1-u)\frac{x_2}{C_2} - \frac{x_4}{RC_2}
\end{aligned} \tag{1}$$

where $x_1 \in \mathbb{R} > 0$, $x_2 \in \mathbb{R} > 0$, $x_3 \in \mathbb{R} > 0$ and $x_4 \in \mathbb{R} > 0$ are the current i_{L1} through inductor L_1, current i_{L2} through inductor L_2, output voltage V_{C1} across capacitor C_1 and the output voltage V_{C2} across the capacitor C_2, respectively. The external input voltage is represented by E and the load by the resistor R. The control input u to the converter is the duty ratio function.

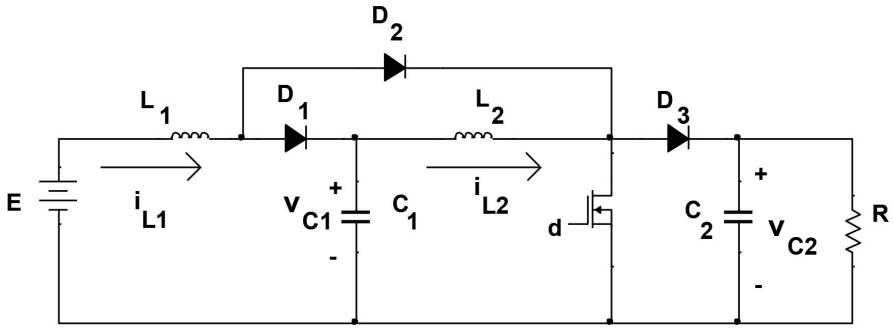

FIGURE 1. Quadratic boost converter

Assuming that the equilibrium of x_4 is $x_{4o} = V_{ref}$ with V_{ref} being the desired output voltage, the solution to the equilibrium point $(x_1, x_2, x_3, x_4, u) = (x_{1o}, x_{2o}, x_{3o}, x_{4o}, u_o)$ is

$$x_{1o} = I_{ref},\ x_{2o} = \sqrt{I_o I_{ref}},\ x_{3o} = \sqrt{V_{ref} E},\ x_{4o} = V_{ref} \tag{2}$$

From (1) and (2), the equilibrium of the control input u is given by

$$u_o = 1 - \sqrt{\frac{E}{V_{ref}}} \tag{3}$$

where $I_{ref} = \frac{V_{ref}^2}{RE}$ and $I_o = \frac{V_{ref}}{R}$.

3. **UDE-Based Controller Design.** In this section, a simple design of the UDE-based controller for the quadratic DC-DC boost converter is presented. From the second equation of (1), we have

$$x_3 = (1-u)x_4 + L_2\dot{x}_2 \tag{4}$$

and from the third equation of (1), we have

$$x_2 = (1-u)x_1 - C_1\dot{x}_3 \tag{5}$$

Substituting (4) and (5) into the first and fourth equations of (1) respectively, we obtain

$$\begin{aligned} \dot{x}_1 &= \frac{u}{L_1}x_4 + f_1(t) \\ \dot{x}_4 &= -\frac{u}{C_2}x_1 + f_2(t) \end{aligned} \tag{6}$$

where

$$f_1(t) = \left(-1 + u - u^2\right)\frac{x_4}{L_1} - (1-u)\frac{L_2}{L_1}\dot{x}_2 + \frac{E}{L_1} \tag{7}$$

and

$$f_2(t) = \left(1 - u + u^2\right)\frac{x_1}{C_2} - (1-u)\frac{C_1}{C_2}\dot{x}_3 - \frac{x_4}{RC_2} \tag{8}$$

It is an easy task to include in the lump signals $f_1(t)$ and $f_2(t)$ the uncertainties of the component values and the unknown parasitics of the converter such as the inductor equivalent series resistances, the MOSFET on-resistance, the diode forward resistances, the conducting voltage of the diodes and the capacitor equivalent series resistances.

Let $e_4 = x_4 - V_{ref}$ and

$$e_1 = x_1 - i_{ref} \tag{9}$$

where i_{ref} is the reference current for the current loop given by

$$i_{ref} = -K_p e_4 - K_i \int_0^t e_4 d\tau \tag{10}$$

with K_p and K_i the proportional and integral gain, respectively. The controller u is designed such that the state error e_1 satisfies the error dynamics equation

$$\dot{e}_1(t) = -\alpha e_1(t) \tag{11}$$

where $\alpha > 0$ is a design parameter. Using (6), (9)-(11) and the fact that $\dot{e}_4 = \dot{x}_4$, the controller u satisfies

$$u\left[\frac{x_4}{L_1} - K_p\frac{x_1}{C_2}\right] = -\alpha e_1(t) - f_1 - K_p f_2 - K_i e_4 \tag{12}$$

The controller u cannot be implemented since f_1 and f_2 are unknown. However, they can be accurately estimated using a low-pass filter such that

$$\hat{f}_1 = f_1 \star g_f(t) \tag{13}$$

and

$$\hat{f}_2 = f_2 \star g_f(t) \tag{14}$$

where '$\star$' is the convolution operator and $g_f(t) = \mathcal{L}^{-1}\{G_f(s)\}$ is the impulse response of the low-pass filter with $G_f(s)$ its transfer function and $\mathcal{L}^{-1}\{.\}$ the inverse Laplace transform operator. Replacing f_1 and f_2 by their estimates $\hat{f}_1$ and $\hat{f}_2$, respectively, we now have

$$u\left[\frac{x_4}{L_1} - K_p\frac{x_1}{C_2}\right] = -\alpha e_1(t) - \hat{f}_1 - K_p\hat{f}_2 - K_i e_4 \tag{15}$$

Substitution of the control action given by (15) into the derivative of (9) and making use of equations in (6) yield the following error dynamics

$$\dot{e}_1(t) = -\alpha e_1(t) + \tilde{f}_1(t) + K_p \tilde{f}_2(t) \tag{16}$$

where $\tilde{f}_1 = f_1 - \hat{f}_1$ and $\tilde{f}_2 = f_2 - \hat{f}_2$ are the estimation errors of the lumped uncertainties. In this work, we consider a strictly proper low-pass filter whose transfer function is

$$G_f(s) = \frac{1}{1+\tau s} \tag{17}$$

where τ is the time constant of the filter. In view of (13), (14) and (17), the estimated errors are

$$\tilde{f}_1 = f_1 \star \mathcal{L}^{-1}\{1 - G_f(s)\},\ \tilde{f}_2 = f_2 \star \mathcal{L}^{-1}\{1 - G_f(s)\} \tag{18}$$

If the filter $G_f(s)$ is designed close to unity over the spectrum of the lumped uncertainties, then we may assume that $\tilde{f}_1 = 0$ and $\tilde{f}_2 = 0$ and from (16) we have

$$\dot{e}_1(t) = -\alpha e_1(t) \tag{19}$$

Using the estimates (13) and (14) with the substitution $f_1 = \left(\dot{x}_1 - u\frac{x_4}{L_1}\right)$ and $f_2 = \left(\dot{x}_4 + u\frac{x_1}{C_2}\right)$ obtained from (6) into the control action (15) yields

$$u\left[\frac{x_4}{L_1} - K_p\frac{x_1}{C_2}\right] = -\alpha e_1(t) - \left(\dot{x}_1 - u\frac{x_4}{L_1}\right) \star g_f - \left(K_p\dot{x}_4 + uK_p\frac{x_1}{C_2}\right) \star g_f - K_i e_4 \tag{20}$$

For any continuous time function $x(t)$, the following relationships [19] hold

$$\begin{aligned} x(t) - x(t) * g_f(t) &= x(t) \star \mathcal{L}^{-1}(1 - G_f(s)) \\ x(t) &= x(t) \star \mathcal{L}^{-1}\left(\frac{1}{1-G_f(s)}\right) \star \mathcal{L}^{-1}(1 - G_f(s)) \\ \dot{x}(t) \star g_f(t) &= x(t) \star \mathcal{L}^{-1}\left(\frac{sG_f(s)}{1-G_f(s)}\right) \star \mathcal{L}^{-1}(1 - G_f(s)) \end{aligned} \tag{21}$$

Using the relationships in (21), the controller given by (20) reduces to

$$\begin{aligned} u = \frac{1}{\left(\frac{x_4}{L_1} - K_p\frac{x_1}{C_2}\right)} \Bigg[&(-K_i e_4 - \alpha e_1) \star \mathcal{L}^{-1}\left(\frac{1}{1-G_f(s)}\right) - x_1 \star \mathcal{L}^{-1}\left(\frac{sG_f(s)}{1-G_f(s)}\right) \\ &- K_p x_4 \star \mathcal{L}_{\prime}^{-1}\left(\frac{sG_f(s)}{1-G_f(s)}\right)\Bigg] \end{aligned} \tag{22}$$

Using (17), the following relationships hold

$$\frac{1}{1-G_f(s)} = 1 + \frac{1}{\tau s};\ \left(\frac{sG_f(s)}{1-G_f(s)}\right) = \frac{1}{\tau} \tag{23}$$

In view of (23) and applying the convolution operator, the UDE-based controller (22) reduces to

$$u = \frac{1}{\left(\frac{x_4}{L_1} - K_p\frac{x_1}{C_2}\right)} \left[(-K_i e_4 - \alpha e_1) - \frac{1}{\tau}K_i\int_0^t e_4 d\tau - \frac{\alpha}{\tau}\int_0^t e_1 d\tau - \frac{x_1}{\tau} - K_p\frac{x_4}{\tau}\right] \tag{24}$$

Using the substitution of $x_1 = e_1 + i_{ref} = e_1 - K_p e_4 - K_i\int_0^t e_4 d\tau$ and $x_4 = e_2 + V_{ref}$ inside the brackets of (24) yields

$$u = \frac{1}{\left(\frac{x_4}{L_1} - K_p\frac{x_1}{C_2}\right)} \left[(-K_i e_4 - \alpha e_1) - \frac{\alpha}{\tau}\int_0^t e_1 d\tau - \frac{e_1}{\tau} - K_p\frac{V_{ref}}{\tau}\right] \tag{25}$$

with $x_1 \in \mathbb{R} > 0$ and $x_4 \in \mathbb{R} > 0$.

Remark 3.1. *In view of (13), (14) and (17), the dynamics of the estimates are*

$$\dot{\hat{f}}_1 = -\frac{\hat{f}_1(t)}{\tau} + \frac{f_1}{\tau},\ \dot{\hat{f}}_2 = -\frac{\hat{f}_2(t)}{\tau} + \frac{f_2}{\tau} \tag{26}$$

From Equation (26) and using $\hat{f}_1 = f_1 - \tilde{f}_1$, $\hat{f}_2 = f_2 - \tilde{f}_2$, the dynamics of the estimation errors are

$$\dot{\tilde{f}}_1 = -\frac{1}{\tau}\tilde{f}_1 + \dot{f}_1,\ \dot{\tilde{f}}_2 = -\frac{1}{\tau}\tilde{f}_2 + \dot{f}_2 \tag{27}$$

In view of (27) and assuming that the derivatives of the lumped uncertainties $\dot{f}_1$ and $\dot{f}_2$ are bounded, the accuracy of the uncertainty estimates requires that the time constant τ of the low-pass filter be as small as possible. However, in practice, its value is determined by the computational capability of the controller and the system noise.

Another way of looking at the estimation using a low-pass filter is the derivation of a reduced observer in the state space form [18]*. We will derive only the estimation of f_1 since the estimation of f_2 will be similar. Using $f_1 = \left(\dot{x}_1 - u\frac{x_4}{L_1}\right)$ into (26), the dynamics of the estimate $\hat{f}_1$ are*

$$\dot{\hat{f}}_1 = -\frac{\hat{f}_1(t)}{\tau} + \frac{1}{\tau}\left(\dot{x}_1 - \frac{ux_4}{L_1}\right) \tag{28}$$

To circumvent the unavailability of the measurement of $\dot{x}_1$, we make the following change of variable

$$z(t) = \hat{f}_1(t) - \frac{x_1}{\tau} \tag{29}$$

Taking the derivative of (29) and using (28) yields the following reduced observer for $f_1(t)$

$$\begin{aligned} \dot{z}(t) &= -\frac{1}{\tau}z(t) - \frac{x_1}{\tau^2} - \frac{ux_4}{\tau L_1} \\ \hat{f}_1(t) &= z(t) + \frac{x_1}{\tau} \end{aligned} \tag{30}$$

However, this reduced observer approach rather than the frequency domain approach will result in a more complicated controller.

4. **Stability Analysis.** In this section, the stability analysis of the quadratic boost converter subject to the controller given by (25) is analyzed and a local stability region is determined in order to adequately select the controller gains.

Using the substitutions $x_1 = e_1 + i_{ref} = e_1 - K_p e_4 - K_i \int_0^t e_4 d\tau$, $x_2 = e_2 + x_{2o}$, $x_3 = e_3 + x_{3o}$ and $x_4 = e_4 + x_{4o}$ into (1) and (25) yields the following equations

$$\begin{aligned} \dot{e}_1 &= -\frac{(1-u)}{L_1}(e_3 + x_{3o}) + K_p\frac{(1-u)}{C_2}(e_2 + x_{2o}) - \frac{K_p}{RC_2}(e_4 + x_{4o}) + K_i e_4 + \frac{E}{L_1} \\ \dot{e}_2 &= -\frac{(1-u)}{L_2}(e_4 + x_{4o}) + \frac{(e_3 + x_{3o})}{L_1} \\ \dot{e}_3 &= \frac{(1-u)}{C_1}(e_1 - K_p e_4 - K_i x_{44}) - \frac{(e_2 + x_{2o})}{C_1} \\ \dot{e}_4 &= \frac{(1-u)}{C_2}(e_2 + x_{2o}) - \frac{(e_4 + x_{4o})}{RC_2} \end{aligned} \tag{31}$$

where

$$u = \frac{1}{\left(\frac{(e_4+x_{4o})}{L_1} - K_p\frac{(e_1 - K_p e_4 - K_i x_{44})}{C_2}\right)}\left[-K_i e_4 - \alpha e_1 - \frac{\alpha}{\tau}x_{11} - \frac{e_1}{\tau} - K_p\frac{V_{ref}}{\tau}\right] \tag{32}$$

with the state variables x_{11} and x_{44} defined as

$$x_{11} = \int_0^t e_1 d\tau,\ x_{44} = \int_0^t e_4 d\tau \tag{33}$$

In this case, we have

$$\dot{x}_{11} = e_1,\ \dot{x}_{44} = e_4 \tag{34}$$

The equilibrium points of x_{11} and x_{44} denoted by x_{11o} and x_{44o} respectively are

$$\begin{aligned} x_{11o} &= -\frac{u_o \tau}{\alpha}\left(\frac{V_{ref}}{L_1} - K_p \frac{I_{ref}}{C_2}\right) - K_p \frac{V_{ref}}{\alpha} \\ x_{44o} &= -\frac{I_{ref}}{K_i} \end{aligned} \tag{35}$$

We define the following errors

$$e_{11} = x_{11} - x_{11o},\ e_{44} = x_{44} - x_{44o} \tag{36}$$

Proving the stability of the overall system is a difficult task. Therefore, the stability analysis will be based on linearization, a classical method adopted in several studies such as in [9].

We define the unique equilibrium point of the system (30) and (33) as $(e_1^*, e_{11}^*, e_2^*, e_3^*, e_4^*, e_{44}^*) = (0, 0, 0, 0, 0, 0)$ and its linearization about the equilibrium is

$$\dot{\tilde{e}} = A\tilde{e} \tag{37}$$

where $\tilde{e}^T = [\tilde{e}_1\ \tilde{e}_{11}\ \tilde{e}_2\ \tilde{e}_3\ \tilde{e}_4\ \tilde{e}_{44}]$ with

$$\begin{aligned} \tilde{e}_1 &= e_1 - e_1^*,\ \tilde{e}_{11} = e_{11} - e_{11}^*,\ \tilde{e}_2 = e_2 - e_2^* \\ \tilde{e}_3 &= e_3 - e_3^*,\ \tilde{e}_4 = e_4 - e_4^*,\ \tilde{e}_{44} = e_{44} - e_{44}^* \end{aligned} \tag{38}$$

and where the matrix A is given by

$$\begin{bmatrix} a\frac{x_{3o}}{L_1} - aK_p\frac{x_{2o}}{C_2} & b\frac{x_{3o}}{L_1} - bK_p\frac{x_{2o}}{C_2} & \frac{K_p}{C_2}(1-u_o) & \frac{(u_o-1)}{L_1} & c\frac{x_{3o}}{L_1} - cK_p\frac{x_{2o}}{C_2} - \frac{K_p}{RC_2} + K_i & d\frac{x_{3o}}{L_1} - dK_p\frac{x_{2o}}{C_2} \\ 1 & 0 & 0 & 0 & 0 & 0 \\ a\frac{V_{ref}}{L_2} & b\frac{V_{ref}}{L_2} & 0 & \frac{1}{L_2} & \frac{(u_o-1)}{L_2} + c\frac{V_{ref}}{L_2} & d\frac{V_{ref}}{L_2} \\ \frac{(1-u_o)}{C_1} - a\frac{I_{ref}}{C_1} & -b\frac{I_{ref}}{C_1} & -\frac{1}{C_1} & 0 & \frac{K_p}{C_1}(u_o-1) - c\frac{I_{ref}}{C_1} & \frac{K_i}{C_1}(u_o-1) - d\frac{I_{ref}}{C_1} \\ -a\frac{x_{2o}}{C_2} & -b\frac{x_{2o}}{C_2} & \frac{1}{C_2}(1-u_o) & 0 & -\frac{1}{RC_2} - c\frac{x_{2o}}{C_2} & -d\frac{x_{2o}}{C_2} \\ 0 & 0 & 0 & 0 & 1 & 0 \end{bmatrix}$$

with

$$\begin{aligned} a &= \frac{\left(-\alpha + \frac{1}{\tau}\right) L_1 C_2 + K_p L_1 u_o}{(C_2 V_{ref} - K_p L_1 I_{ref})} \\ b &= \frac{-\frac{\alpha L_1 C_2}{\tau}}{(C_2 V_{ref} - K_p L_1 I_{ref})} \\ c &= \frac{-K_i L_1 C_2 - \left(C_2 + K_p^2 L_1\right) u_o}{(C_2 V_{ref} - K_p L_1 I_{ref})} \\ d &= \frac{-K_p K_i L_1 u_o}{(C_2 V_{ref} - K_p L_1 I_{ref})} \end{aligned} \tag{39}$$

The system (37) is stable if the eigenvalues of the matrix A computed as

$$|sI - A| = 0 \tag{40}$$

lie in the open left-hand s plane with s being the complex variable.

Since the effectiveness of the proposed controller will be compared against the robust sliding-mode controller proposed in [9], the parameters of the converter used in [9] are therefore considered in the simulation for consistency. They are given as

$$\begin{aligned} &L_1 = 120\ \mu\text{H},\ L_2 = 4.7\ \text{mH},\ C_1 = C_2 = 9\ \mu\text{F} \\ &R = 8000\ \Omega,\ E = 25\ \text{V},\ V_{ref} = 400\ \text{V} \end{aligned} \tag{41}$$

Using (37)-(41), the evaluation of the stability region in the $K_p - K_i$ plane is given in Figure 2.

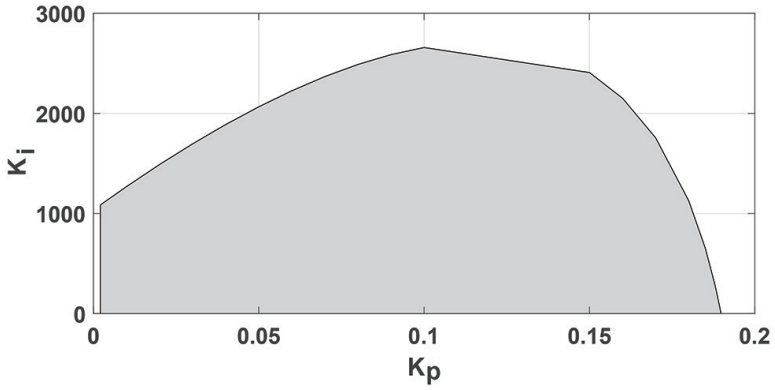

FIGURE 2. Evaluation of the stability region

5. **Effects of the Controller Parameters on the Output Transient.** The implementation of the controller given by (25) requires the proper selection of α, τ, K_p and K_i. Many simulations were performed to investigate their effect on the transient output response. This section presents simple tuning guidelines of the gains in order to obtain a satisfactory output response.

1) The decay rate α of the error dynamics of $e_1(t)$ given by Equation (19) should be selected high enough to ensure that the motion rate of the current is much faster than the motion rate of the output voltage. To this end, we may select

$$\alpha \geq \frac{10}{RC_2} \tag{42}$$

2) The accuracy of the uncertainty estimates requires that the time constant τ of the low-pass filter to be as small as possible. However, in practice, its value is determined by the computational capability of the controller and the system noise.

3) The effect of the proportional gain K_p and the integral gain K_i that define the reference current given in (10) on the output response are individually investigated using Matlab/Simulink with the following observations:

For a given value of K_p, an increase in K_i reduces the settling time after the onset of load and input voltage step changes with a minimum effect on the output overshoot. However, as the value of K_i increases, the percent overshoot during start-up output transient increases. Therefore, there is a trade-off between the recovery time after input and load disturbances and the overshoot of the start-up output transient.

Keeping K_i constant, an increase in K_p reduces the overshoot during load and input changes with a minimum effect on the recovery time. However, as the value of K_p increases, there is the possibility of small steady-state oscillations at the output voltage. Based on these observations, the following tuning guideline for the selection of K_p and K_i is proposed as:

Select the maximum gain K_p that ensures the stability of the system (37) and select $K_i = 0$. If the output voltage response is satisfactory with no steady state oscillations, then increase K_i to reduce the recovery time due to external disturbances until a maximum prespecified percent overshoot during start-up output transient is reached. On the other hand, if the output response exhibits small steady state oscillations for maximum K_p with $K_i = 0$, then reduce K_p until a smoother satisfactory output response is achieved. Accordingly, adjust K_i until the maximum allowable overshoot is achieved for the start-up output transient.

6. **Comparison Simulation with Sliding Mode Control.** A Matlab/Simulink simulation is performed to compare the robust sliding-mode controller in [9] with the proposed controller for the quadratic boost converter whose parameters are given in (41).

The SMC proposed in [9] is

$$u = 0.5(1 - sign(S)) \tag{43}$$

where the switching manifold S is given by

$$S = x_1 - I_E(t) \tag{44}$$

with

$$I_E(t) = -K_p(x_4(t) - V_{ref}) - K_i \int_{-\infty}^{t} (x_4(\lambda) - V_{ref})\, d\lambda \tag{45}$$

The PI gains are determined to be $K_p = 0.0268$ and $K_i = 13.3$.

For the UDE-based controller, a PWM modulator with a switching frequency of 100 kHz is used. The parameters of the UDE controllers are chosen using the tuning guidelines of Section 5.

From (41) and (42), the decay rate is $\alpha \geq 130$. In this simulation, $\alpha = 250$ is chosen. For a simulation sampling time of 0.1 μs, the filter time constant is appropriately chosen as $\tau = 5$ μs. The maximum gain K_p to ensure stability of the system (37) is $K_p = 0.18$. With this gain, the output exhibited a small steady state output oscillations. The gain was reduced to $K_p = 0.1$ for a smoother response. The gain K_i was increased to $K_i = 30$, to meet the maximum permissible overshoot of 20% used in this simulation. Please note that K_i should be high enough to reduce the recovery time during input and load disturbances but not too high to cause unacceptable transient output overshoots. In summary, the parameters of the controller are

$$\alpha = 250,\ \tau = 5\ \mu\text{s},\ K_p = 0.1,\ K_i = 30 \tag{46}$$

As in [9], input and load variations as well as reference voltage steps are applied to the converter in the extreme values of the converter operational range.

6.1. **Output power disturbance rejection.** Figure 3 shows the simulation plot of the output response due to load variations. In this case, a step disturbance of 62.5 mA (25% of the nominal load) is applied to the converter operating at different equilibrium points. The maximum voltage deviation is 2%, and the disturbance is completely rejected in less than 29 ms. Using the controller proposed in [9], the maximum voltage deviation reported is 4.9% and the disturbance is completely rejected in less than 72 ms.

6.2. **Input voltage disturbance rejection.** Figure 4 shows the simulation plot of the output response due to input voltage disturbance. In this case, a step input voltage of +5 V is applied to the converter if the initial input voltage is 15 V and a step of −5 V if the initial voltage is 25 V. It is seen from Figure 4 that the maximum voltage deviation is

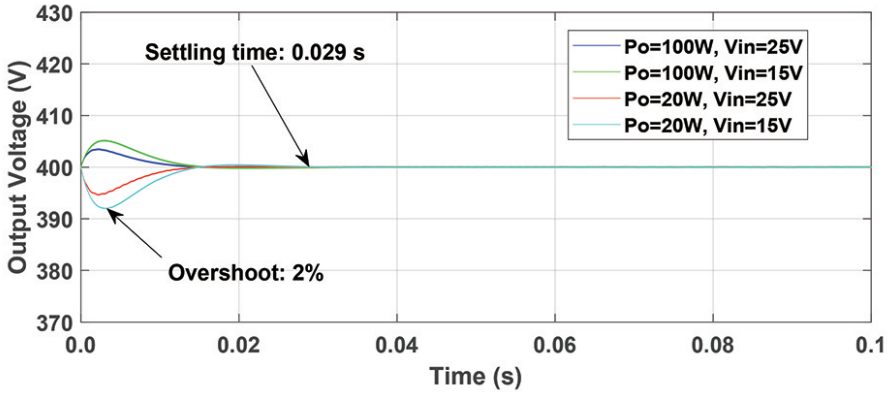

FIGURE 3. Transient response to output power step disturbances in the extreme values of the converter operational range

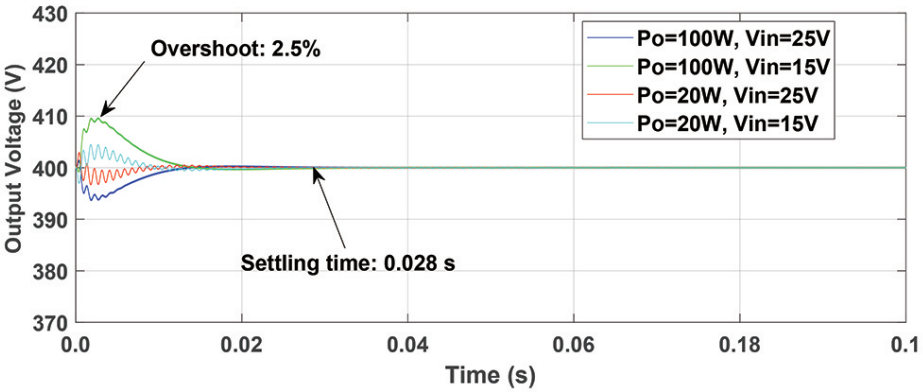

FIGURE 4. Transient response with input voltage step disturbances in the extreme values of the converter operational range

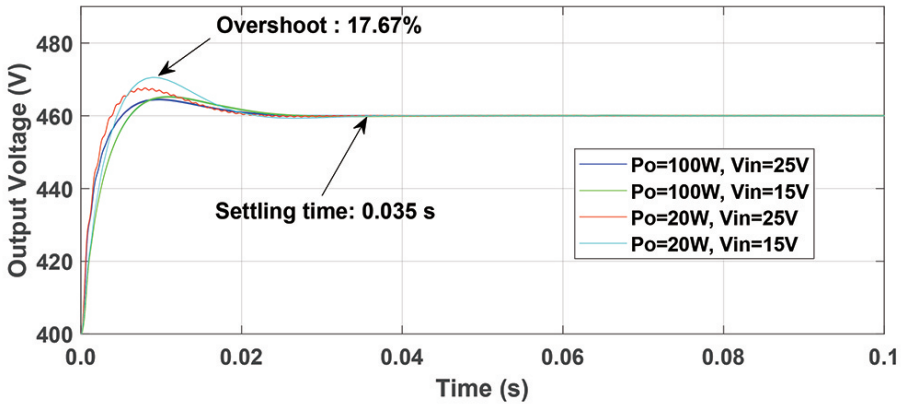

FIGURE 5. Transient response to a voltage step change in the extreme values of the converter operational range

2.5% and the disturbance is completely rejected in less than 28 ms. In [9], the maximum voltage deviation reported is 5.4%, and the disturbance is completely rejected in less than 62 ms.

6.3. **Set-point change transient response.** Figure 5 shows the simulation plot of the output response due to a reference voltage step of 60 V from a regulated output voltage

of 400 V. It is seen from Figure 5 that the overshoot is 17.67% and the settling time is approximately 35 ms. In [9], the overshoot reported is 45% and the settling time is approximately 72 ms.

Please note that the region of stability given in Figure 2 is larger than the one defined in [9] that shows that the system is stable for much smaller values of K_p and therefore, limits the choice of the proportional gain for a better performance of the system.

7. **Simulation and Experimental Results.** In this section, some simulation and experimental results are performed to validate the robustness of the proposed controlled in the regulation of the quadratic boost converter subject to input and load disturbances. The parameters of a 2-W prototype of the quadratic boost converter are considered in these experiments and they are

$$L_1 = 180\ \mu\text{H},\ L_2 = 1\ \text{mH},\ C_1 = C_2 = 20\ \mu\text{F},\ R = 1000\ \Omega,\ E = 6\ \text{V},\ V_{ref} = 20\ \text{V} \quad (47)$$

7.1. **Simulation results.** The parameters of the controller (25) are selected based on the tuning guidelines of Section 5. From (41) and (42), the decay rate is $\alpha \geq 500$. In this experiment, $\alpha = 1000$ is chosen. The accuracy of the uncertainty estimates requires that the time constant τ of the low-pass filter to be as small as the computational capability of the controller allows it. The dSPACE 1104 real-time controller board used in this experiment limits τ to be no less than 50 μs. The maximum gain K_p to ensure stability of the system (37) is $K_p = 0.38$. With this gain, the output exhibited large steady state output oscillations. The gain was reduced to $K_p = 0.1$ for a smoother response. The gain K_i was increased to $K_i = 30$ to meet the maximum permissible overshoot of 20% used in this experiment. In summary, the parameters of the controller are

$$\alpha = 1000,\ \tau = 50\ \mu\text{s},\ K_p = 0.1,\ K_i = 30 \quad (48)$$

To perform the simulation, we assume that the input voltage E varies from $E = 6$ V to $E = 4$ V at $t = 0.1$ s and from $E = 4$ V to $E = 6$ V at $t = 0.2$ s. The load resistor R varies stepwise from $R = 1000\ \Omega$ to $R = 500\ \Omega$ at $t = 0.3$ s and then back to $R = 1000\ \Omega$ at $t = 0.4$ s. Finally, the reference voltage V_{ref} is changed from 20 V to 30 V at $t = 0.6$ s.

From the plot of the transient output voltage depicted in Figure 6, the output voltage undergoes a maximum voltage deviation of 5% when the input E changes from 6 V to 4 V and then back to 6 V with the input disturbance completely rejected in less than 20 ms. There is a maximum output voltage deviation of 1.6% when the load resistor R varies

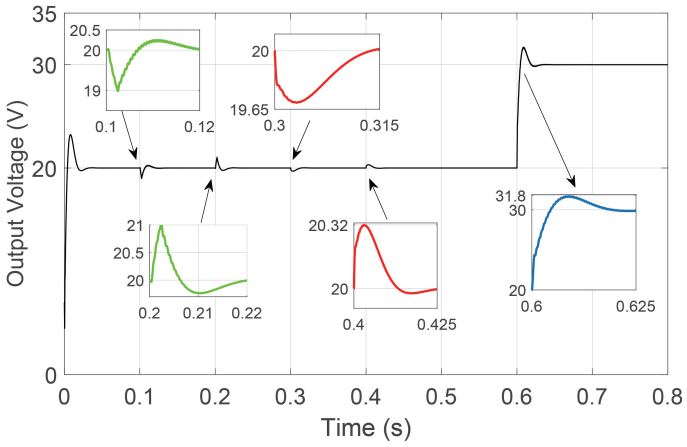

FIGURE 6. Output voltage transient response to input, load and voltage reference changes

stepwise periodically between 1000 Ω and 500 Ω with the load disturbance completely rejected in less than 25 ms. The output voltage exhibits a percent overshoot of 18% with a settling time less than 25 ms during a reference voltage change V_{ref} from 20 V to 30 V.

7.2. **Experimental results.** Using the controller (25) with the same parameters as the simulation and given in (48), the experimental results are depicted in Figures 7 through 12. Figure 7 shows the response due to a step change of the reference voltage V_{ref} from 20 V to 30 V. In this case, the percent overshoot is 20% and the settling time is less than 30 ms. Figure 8 depicts the robustness of the UDE-based controller to step load variations and Figure 9 is a zoom in. In this case, the load resistor R varies stepwise periodically between 1000 Ω and 500 Ω with $V_{ref} = 20$ V. The voltage deviation is 2.5%, and the disturbance is rejected in less than 20 ms. Shown in Figure 10 is the robustness of the controller to an external input voltage disturbance where E undergoes a change from 6 V to 4 V and then back to 6 V with Figure 11 and Figure 12 depicting zoom ins when the input undergoes a change from 6 V to 4 V and from 4 V to 6 V, respectively. In this case, the maximum voltage deviation is 4%, and the disturbance is rejected in less than 25 ms. Table 1 summarizes the maximum percent overshoot and the maximum settling time using the experimental results and the simulation results for the input and load

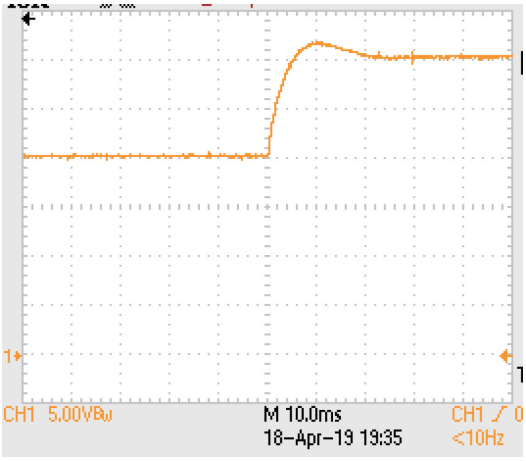

FIGURE 7. Output response (5 V/div, 10 ms/div) with step reference voltage change from 20 V to 30 V

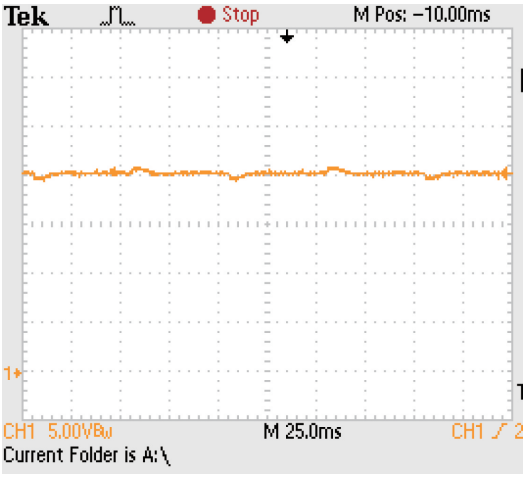

FIGURE 8. Output response (5 V/div, 25 ms/div) with the load resistor R varying periodically stepwise between 1000 Ω and 500 Ω

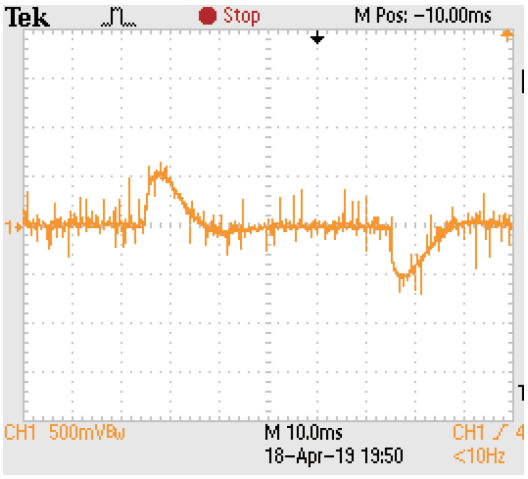

FIGURE 9. Zoom in of Figure 8 (0.5 V/div, 10 ms/div)

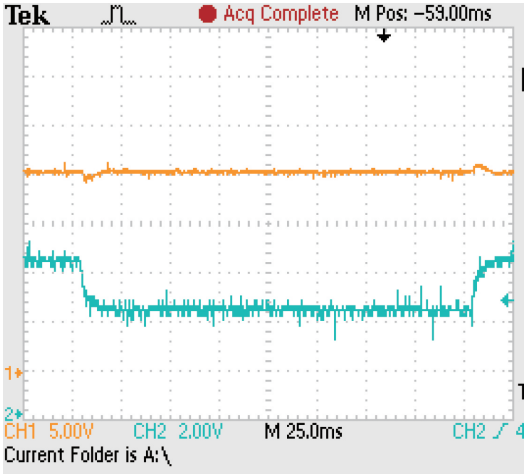

FIGURE 10. Output response with the input voltage E undergoing a change from 6 V to 4 V then back to 6 V. Top: Output voltage (5 V/div, 25 ms/div); Bottom: Input voltage E (2 V/div, 25 ms/div).

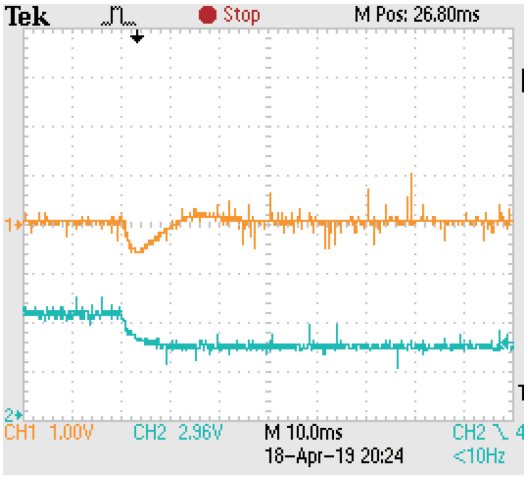

FIGURE 11. Zoom in of Figure 10 with the input voltage E undergoing a step change from 6 V to 4 V. Top: Output voltage (1 V/div, 10 ms/div); Bottom: Input voltage E (2.96 V/div, 10 ms/div).

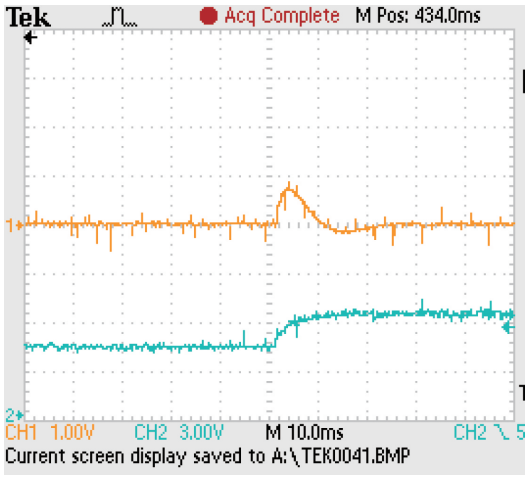

FIGURE 12. Zoom in of Figure 10 with the input voltage E undergoing a change from 4 V to 6 V. Top: Output voltage (1 V/div, 10 ms/div); Bottom: Input voltage E (3 V/div, 10 ms/div).

TABLE 1. Maximum percent overshoots and maximum settling times for experimental and simulation (in parenthesis) results

Type of disturbances	PO (%)	T_s (ms)
Input voltage disturbance	4 (5)	25 (20)
Load disturbance	2.5 (1.6)	20 (25)
Reference voltage change	20 (18)	30 (25)

disturbances and the voltage reference change. Please note that the simulation results are given in parenthesis.

There is a good agreement between the experimental results and the simulation results. The small disparities are due to parasitics and other nonlinearities of the converter model used in the simulation.

8. **Conclusion.** A robust UDE-based controller is designed to regulate the output voltage of the quadratic boost converter. The uncertainties and disturbances are lumped into an unknown signal that is accurately approximated using a low-pass filter of sufficiently large bandwidth and the estimate is utilized by the controller to cancel their effect and tightly regulate the converter output voltage. The proposed controller is simple in its design and yet exhibits good performance in the presence of disturbances. Its robustness is validated by computer simulation and experimental results. Future work will be the development of a simpler procedure to systematically determine the controllers parameters to meet certain specifications and to perform the stability analysis of the non-linear closed-loop system instead of the linearized one.

Acknowledgment. The authors gratefully acknowledge the helpful comments and suggestions of the reviewers, which have improved the presentation.

REFERENCES

[1] M. A. Khan, A. Ahmed, I. Husain, Y. Sozer and M. Badawy, Performance analysis of bidirectional DC-DC converters for electric vehicles, *IEEE Transactions on Industry Applications*, vol.51, no.4, pp.3442-3452, DOI: 10.1109/TIA.2015.2388862, 2015.

[2] S. Chakraborty et al., DC-DC converter topologies for electric vehicles, plug-in hybrid electric vehicles and fast charging stations: State of the art and future trends, *Energies*, vol.12, no.4, DOI: 10.3390/en12081569, 2019.

[3] L. Callegaro, M. Ciobotaru, D. J. Pagano and J. E. Fletcher, Feedback linearization control in photovoltaic module integrated converters, *IEEE Transactions on Power Electronics*, vol.34, no.7, pp.6876-6889, DOI: 10.1109/TPEL.2018.2872677, 2019.

[4] B. Housseini, A. F. Okou and R. Beguenane, Robust nonlinear controller design for on-grid/off-grid wind energy battery-storage system, *IEEE Transactions on Smart Grid*, vol.9, no.6, pp.5588-5598, DOI: 10.1109/TSG.2017.2691707, 2018.

[5] C. A. Soriano-Rangel, W. He, F. Mancilla-David and R. Ortega, Voltage regulation in buck-boost converters feeding an unknown constant power load: An adaptive passivity-based control, *IEEE Transactions on Control Systems Technology*, vol.29, no.1, pp.395-402, DOI: 10.1109/TCST.2019.2959535, 2021.

[6] J. A. Morales-Saldana, R. Galarza-Quirino, J. Leyva-Ramos, E. E. Carbajal-Gutierrez and M. G. Ortiz-Lopez, Multiloop controller design for a quadratic boost converter, *IET Electric Power Applications*, vol.1, no.3, pp.362-367, DOI: 10.1049/iet-epa:20060426, 2007.

[7] J. Leyva-Ramos, M. G. Ortiz-Lopez, L. H. Diaz-Saldierna and J. A. Morales-Sandana, Switching regulator using a quadratic boost converterfor wide DC conversion ratios, *IET Power Electronics*, vol.2, no.5, pp.605-613, DOI: 10.1049/iet-pel.2008.0169, 2009.

[8] J. A. Morales-Saldana, R. Loera-Palomo, E. Palacios-Hernandez and J. L. Gonzaz-Martinez, Modelling and control of a DC-DC quadratic boost converter with R2P2, *IET Power Electonics*, vol.7, no.1, pp.11-22, DOI: 10.1049/iet-pel.2012.0749, 2014.

[9] O. Lopez-Santos, L. Martinez-Salamero, G. Garcia, H. Valderrama-Blavi and T. Sierra-Polanco, Robust sliding-mode control design for a voltage regulated quadratic boost converter, *IEEE Transactions on Power Electronics*, vol.30, no.4, pp.2313-2327, DOI: 10.1109/TPEL.2014.2325066, 2015.

[10] S. H. Chincholkar and C.-Y. Chan, Design of fixed-frequency pulsewidth-modulation-based sliding-mode controllers for the quadratic boost converter, *IEEE Transactions on Circuits and Systems II: Express Briefs*, vol.64, no.1, pp.51-55, DOI: 10.1109/TCSII.2016.2546902, 2017.

[11] W. Jiang, S. H. Chincholkar and C.-Y. Chan, Comparative study of adaptive current-mode controllers for a hybrid-type high-order boost converter, *IET Power Electronics*, vol.11, no.3, pp.524-530, DOI: 10.1049/iet-pel.2016.1045, 2018.

[12] W. Jiang, S. H. Chincholkar and C.-Y. Chan, Modified voltage-mode controller for the quadratic boost boost converter with improved output performance, *IET Power Electronics*, vol.11, no.14, pp.2222-2231, DOI: 10.1049/iet-pel.2018.5037, 2018.

[13] S. Oucheriah, Robust adaptive output feedback controller for a quadratic boost converter, *ICIC Express Letters, Part B: Applications*, vol.10, no.9, pp.789-795, 2019.

[14] A. Francesco et al., Nonlinear robust control of a quadratic boost converter in a wide operation range, based on extended linearization method, *Electronics*, vol.11, no.2336, DOI: 10.3390/electronics 11152336, 2022.

[15] S. Chincholkar, M. Tariq and S. Urooj, Large-signal stability of the quadratic boost converter using a disturbance observer-based sliding-mode control, *Mathematics*, vol.11, no.18, 3945, https://www.mdpi.com/2227-7390/11/18/3945, 2023.

[16] S. Oucheriah, Current-sensorless robust sliding mode control for a quadratic boost converter, *TechRxiv*, DOI: 10.36227/techrxiv.171994682.26484582/v1, 2024.

[17] Q. C. Zhong and D. Rees, Control of uncertain LTI systems based on an uncertainty and disturbance estimator, *Transactions of the ASME, Jounal of Dynamic Systems, Measurement and Control*, vol.126, no.4, pp.905-910, DOI: 10.1115/1.1850529, 2004.

[18] A. Castillo, R. Sanz, P. Garcia and P. Albertos, Robust design of the uncertainty and disturbance estimator, *IFAC-PapersOnLine*, vol.50, no.1, pp.8262-8267, DOI: 10.1016/j.ifacol.2017.08.1396, 2017.

[19] S. Oucheriah, Robust control of the DCDC boost converter based on the uncertainty and disturbance estimator, *International Journal of Electronics*, vol.104, no.11, pp.1810-1822, DOI: 10.1080/00207217.2017.1326529, 2017.

Author Biography

Said Oucheriah received the B.S. degree in Electrical Engineering from Case Western Reserve University, Cleveland, Ohio, an M.S. degree and a Ph.D. degree in Electrical Engineering from Cleveland State University, Cleveland, Ohio in 1981, 1983 and 1987, respectively. He is a Professor Emeritus at Northern Illinois University, DeKalb, Illinois where he has been teaching for over 32 years. His research interests include time-delay systems, control of large scale systems and robust adaptive control.

Abul Azad is a Professor in the College of Engineering and Engineering Technology at Northern Illinois University in the US. He received his B.S. degree and an M.S. degree in Electronics Engineering, University of Dhaka, Bangladesh in 1984 and 1987, respectively, and his Ph.D. degree in Control and Systems Engineering from University of Sheffield, UK in 1994. With over 40 years in academia, his research focuses on the Internet of Things, remote laboratories, mechatronic systems, mobile robotics, and educational research. Dr. Azad is a member of the editorial boards for multiple professional journals and actively participates in various professional organizations, including IEEE, IET, ASEE, ISA, IAOE, and the CLAWAR Association. He has chaired numerous conferences and workshops in these fields. Additionally, he has served as a program evaluator for ABET and is involved in assessing research and development projects for funding agencies across the U.S., Europe, and Australia.